International Journal of Remote Sensing

ISSN: (Print) (Online) Journal homepage: www.tandfonline.com/journals/tres20

Application and comparison of remote sensing techniques for data-driven disaster debris quantification

Jasmine H. Bekkaye & Navid H. Jafari

To cite this article: Jasmine H. Bekkaye & Navid H. Jafari (2024) Application and comparison of remote sensing techniques for data-driven disaster debris quantification, International Journal of Remote Sensing, 45:8, 2808-2831, DOI: 10.1080/01431161.2024.2339197

To link to this article: https://doi.org/10.1080/01431161.2024.2339197

Published online: 11 Apr 2024.

INTERNATIONAL JOURNAL OF REMOTE SENSING
2024, VOL. 45, NO. 8, 2808–2831
https://doi.org/10.1080/01431161.2024.2339197

Taylor & Francis
Taylor & Francis Group

Application and comparison of remote sensing techniques for data-driven disaster debris quantification

Jasmine H. Bekkaye and Navid H. Jafari

Department of Civil and Environmental Engineering, Louisiana State University, Baton Rouge, USA

ABSTRACT

Effective disaster debris management requires reasonable predictions pre-hazard and estimates post-hazard of debris for a community to get back to normal sooner. However, there is a lack of data related to post-disaster waste quantities that could validate and improve debris predictions. This knowledge gap can be addressed by using remote sensing technology to quantify disaster debris promptly following a hazard. This study aimed to demonstrate and compare multiple remote sensing tools available for quantifying disaster debris using post-disaster data collected following Hurricane Ida. The tools used in this study are satellite imagery, emergency response airborne imagery, unmanned aerial vehicles (UAVs), and terrestrial laser scanning (TLS). We found that satellite imagery is useful for quantifying vegetative debris generation and transportation across vast areas, however it is often limited by spatial and temporal resolutions. Emergency response airborne imagery, collected within days following the hazard, is well-suited for quantifying transported vegetative debris and can assist debris clearance of emergency service routes across large areas, although it can be limited spatially and temporally to the interests of the acquiring agency. UAVs and TLS can provide precise volumes of debris but UAVs may be a better option due to their lower cost and computational demand. Guidance is provided for selecting a remote sensing tool based on the desired application and available resources, which can assist decision making for disaster waste managers.

ARTICLE HISTORY
Received 20 July 2023
Accepted 19 March 2024

KEYWORDS
Disaster debris; disaster waste management; UAV; terrestrial lidar; photogrammetry

1. Introduction

Natural hazards generate tremendous amounts of disaster debris streams that subsequently cause cascading economic, social, and environmental losses and impact response and recovery efforts (Brown, Milke, and Seville 2011; Luther 2017). Disaster debris removal is laborious, and inadequate management results in increased costs, clean-up delays, and adverse environmental and human health consequences (Brown, Milke, and Seville 2011; Luther 2017; USEPA 2019). An effective disaster debris management plan requires reasonable predictions of the type, quantity, and location of debris that will be generated by the hazard to efficiently deploy response and recovery resources (FEMA 2007; USEPA 2019). Additionally, debris predictions are necessary to determine the size and number of

CONTACT Jasmine H. Bekkaye jbekka1@lsu.edu Department of Civil and Environmental Engineering, Louisiana State University, 3504 Patrick Taylor Hall, Baton Rouge, LA 70803, USA

required Temporary Debris Managements Sites (TDMS), or temporary locations where disaster debris is stored until it is reduced in volume and/or taken to a final disposition site (FEMA 2007; NASEM 2014). However, there is a lack of data collected during and post-disaster of waste quantities to validate and improve pre-disaster debris predictions (Brown, Milke, and Seville 2011; Jalloul et al. 2022).

The state-of-the-art in evaluating debris quantities are summarized in Marchesini et al. (2021), and Zhang et al. (2019) and can primarily be divided into predictive statistical models, technology-based observational tools, such as remote sensing, or a combination of these. Multiple federal agencies have developed statistical debris estimation models that are primarily based on type and severity of the hazard (e.g. hurricane intensity, earthquake magnitude) and characteristics of the affected area (e.g. square footage of buildings, building/tree/population density) (Marchesini, Beraud, and Barroca 2021; F. Zhang et al. 2019). However, statistical models can be off by orders of magnitude due to their generality and inherent uncertainty (Bekkaye and Jafari 2023; Marchesini, Beraud, and Barroca 2021). Many statistical models are heavily dependent on national or regional databases and are developed from historical data, which may not be available in many countries and limits the ability of those countries to apply existing statistical models for their location or develop their own estimation methods (Marchesini, Beraud, and Barroca 2021). Additionally, many statistical models are unable to account for the variety in types of waste material in disaster debris, which can drastically differ in mass and volume, increasing the uncertainty of estimates (Marchesini, Beraud, and Barroca 2021). Statistical methods are further limited by the lack of post-disaster waste quantities to validate estimations. Efforts have been made to collect post-disaster waste quantities more accurately. For example, Jafari et al. (2019) acquired post-disaster waste data collected from the monitor consultants hired to remove debris in Beaumont, Texas, U.S.A., following Hurricane Harvey in 2017. However, post-disaster waste tonnage linked to origin location is often unavailable and inconsistent as emergency management officials work to remove debris in a timely manner (Brown, Milke, and Seville 2011; F. Zhang et al. 2019). This problem can be alleviated by quantifying debris in the midst of a disaster using remote sensing technologies.

Remote sensing technology such as satellite imagery, airborne (airplane) imagery, unmanned aerial vehicle (UAV) imagery, and lidar can be used to spatially identify and quantify debris. These tools assist in areas without historical post-disaster waste data (Marchesini, Beraud, and Barroca 2021; F. Zhang et al. 2019) and provide an alternative for estimating debris quantities when ground-truthed post-disaster waste data is unavailable. Optical satellite, airborne, or UAV imagery can be utilized to identify and measure the spatial extent and location of damage and debris, and countless studies have explored these tools for various disasters and locations. For instance, Jiang and Friedland (2016) utilize IKONOS panchromatic satellite and National Oceanic and Atmospheric Administration (NOAA) emergency response airborne imagery to detect building damage debris zones following Hurricane Katrina in 2005. Similarly, Shirai et al. (2016) utilize RapidEye satellite imagery acquired before and after the Great East Japan Earthquake and Tsunami in 2011 to estimate the disaster building domain. To estimate vegetative debris (tree stumps, branches, trunks, and other leafy material) from downed trees, Szantoi et al. (2012) couple post-event airborne imagery with statistical modelling from tree stem diameter-volume bulking factors and field measured estimates of downed tree

debris volume. Satellite imagery alone can provide a quick evaluation of damage and debris across large areas. However, they are affected by cloud cover, spatial resolution, and acquisition is limited temporally depending on the satellite. Several similar studies have been conducted on damage and debris detection using just UAV imagery (e.g. Hanifa et al. 2022; Yeom et al. 2019), a combination of satellite and UAV imagery (e.g. Ghaffarian and Kerle 2019; Kakooei and Baleghi 2017), and a combination of airborne imagery and lidar (e.g. Pham et al. 2014). These studies primarily detect damage and debris in imagery using image classification techniques and more recently deep learning techniques (e.g. Chowdhury et al. 2020; Duarte et al. 2018; Hamdi, Brandmeier, and Straub 2019; Hong et al. 2022; Pi, Nath, and Behzadan (2020a, 2020b); Wang et al. 2021). The numerous studies using UAV imagery have primarily focused on damage and debris detection rather than debris quantification. The chaotic nature of disaster recovery operations presents challenges for debris quantification, such as deploying to locations with accumulated disaster debris, deploying at the right time because debris moves quickly (e.g. from homes to curbsides, curbsides to TDMS), safety and access concerns due to unstable structures, blocked infrastructure, and hazardous conditions, and coordinating with emergency managers without disrupting their operations.

Point clouds produced by lidar or photogrammetry provide elevation and volume information, making the technique extremely suitable for disaster debris volume estimation. In 2007, lidar was employed by the United States Geological Survey (USGS) to estimate debris volumes from Hurricane Katrina in coastal Mississippi, U.S.A., using a combination of NOAA emergency response imagery and airborne lidar data (Hansen et al. 2007). This approach performs image classification to identify locations with debris and subsequently uses the lidar data to measure debris volumes (Hansen et al. 2007). Similarly, Labiak et al. (2011) utilize post-disaster airborne lidar data to quantify building damage and debris in Port-au-Prince, Haiti following the 2010 earthquake, and Axel et al. (2016) employ post-disaster airborne lidar data to quantify roadway debris. These tools are able to swiftly quantify debris prior to being collected and brought to TDMS. Koyama et al. (2016) utilize Synthetic Aperture Radar (SAR) data to estimate the volume of debris brought to a TDMS following the Great East Japan Earthquake and Tsunami, demonstrating another approach for quantifying debris volumes. Another potential lidar tool is terrestrial laser scanning (TLS). TLS can be advantageous over airborne lidar due to its higher point densities, portability for more frequent surveys, and applications for surveying sides of buildings or objects that may be obscured from aerial view such as in urban environments. TLS for disaster management has primarily focused on structural damage assessments following a hazard, e.g. 2008 Wenchuan earthquake in China (Dai et al. 2018; Jiao, Jiang, and Li 2019), 2010 Chile Earthquake and Tsunami (Olsen et al. 2012), and Hurricane Michael in 2018 (Berman et al. 2020). Acquisition and access to SAR, airborne lidar, and TLS data near the time of a disaster is typically constrained by cost and logistics (Jalloul et al. 2022).

UAVs can provide an alternative to post-event SAR and lidar and are less limited by spatial and temporal resolutions compared to satellite imagery, although spatial limitations still exist due to airspace restrictions and flight time. Nonetheless, they can still serve as a feasible option for estimating waste volumes at the roadside curb and disposal facilities. Saffarzadeh et al. (2017, 2019) employ UAVs to quantify disaster debris volumes at TDMS following earthquakes in Japan in 2016 and Iran in 2017. Son et al. (2019) and Yoo

et al. (2017) propose methods and optimal UAV parameters for estimating disaster waste volumes by using landfills as a testbed. Filkin et al. (2022) and Sliusar et al. (2022) estimate waste quantities at landfills but during normal operations and not by disasters.

The frequency of disaster events and their impacts is increasing (CRED 2022; NOAA 2022), highlighting the growing need to further establish the feasibility of using remote sensing tools to quantify disaster debris during the response and recovery phases. This should be investigated across the variety of hazards (wildfires, floods, windstorms, coastal storms, landslides, earthquakes) because each hazard creates different debris types (FEMA 2007; USEPA 2019). Furthermore, collecting post-disaster debris quantities has been identified as a high priority for sustainable disaster debris management (Jalloul et al. 2022) and more standardized workflows need to be established for using remote sensing technologies to quantify debris. Although several studies have been performed using remote sensing technologies to quantify disaster debris, no studies have been found that apply and compare the effectiveness and performance of multiple technologies. To our knowledge, no studies were found beyond Saffarzadeh et al. (2017, 2019) that utilize UAVs to estimate disaster debris volumes at TDMS. Additionally, no studies were found that use TLS to estimate debris volumes at TDMS. As a result, the objective of this study is to demonstrate and compare multiple remote sensing tools available for quantifying disaster debris using post-disaster data collected following Hurricane Ida in 2021, including UAV and TLS data collected at a TDMS. The tools used in this study are satellite imagery, emergency response airborne imagery, UAV, and TLS, and were selected based on their ease of access for disaster management contexts and availability to the authors at the time of the disaster. This approach aims to ascertain the appropriate application of each tool based on performance metrics (time for fieldwork, time for processing raw data, time for quantitative analyses, spatial coverage, spatial resolution, temporal resolution, cost, and operational effort) and provide recommendations for selecting one or multiple tools for debris quantification based on the desired application and available resources.

2. Materials and methods

2.1. Study area and hazard

Hurricane Ida made landfall on 29 August 2021 in southeastern Louisiana, U.S.A., near the town of Port Fourchon as a Category 4 hurricane on the Saffir-Simpson scale (wind speeds of 58.5–69.3 m/s) (Beven, Hagen, and Berg 2022). Hurricane Ida underwent rapid intensification as it approached the Louisiana coast, reaching maximum sustained windspeeds of 67 m/s (150 mph) at landfall (Beven, Hagen, and Berg 2022). The heaviest precipitation was concentrated on the eastern side of the storm, resulting in over 25.4 cm (10 in) of precipitation over portions of southeastern Louisiana and storm surge flooding up to 3 m (10 ft) between Golden Meadow and Grand Isle, Louisiana (Beven, Hagen, and Berg 2022). Southeastern Louisiana, primarily the Barataria Basin, was chosen as a testbed for this study due to the tremendous amount of wind and flood damage and resulting debris generated. As part of a collaborative National Science Foundation (NSF) Nearshore Extreme Events Reconnaissance (NEER) and Geotechnical Extreme Events Reconnaissance (GEER) Associations effort, a weeklong deployment was conducted in southeast Louisiana from October 10 to 15 to assess the extent and impact of damage,

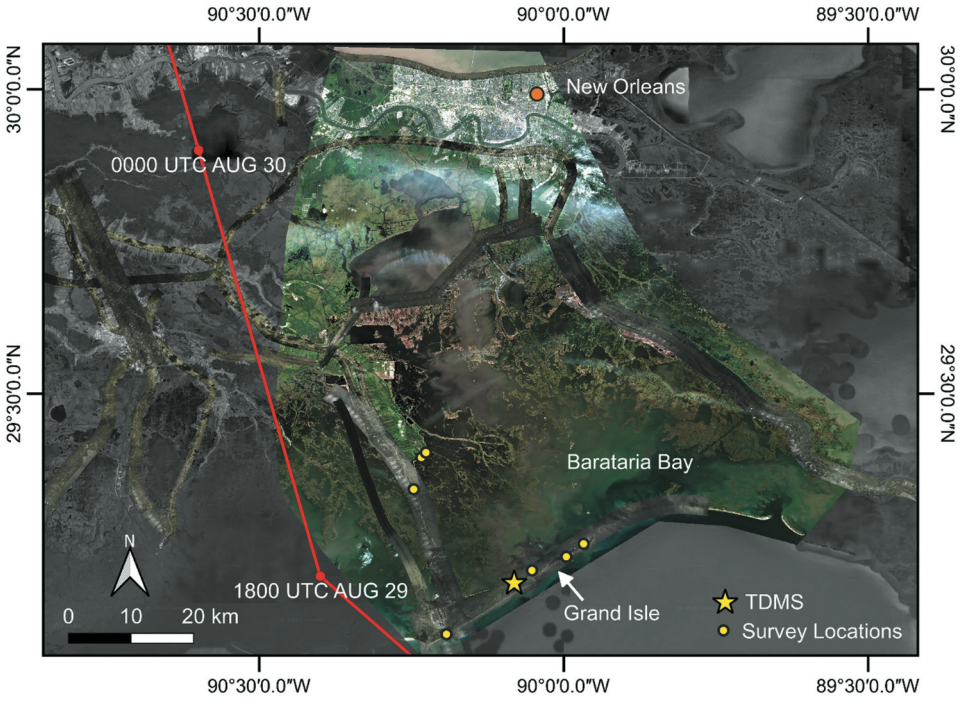

Figure 1. Study area, survey locations, TDMS, and time-stamped (UTC) path of the center of Hurricane Ida, overlaid with Sentinel-2 satellite (colourized map) and NOAA airborne (colourized, rectangular swaths) imagery used in the study. (Basemap: ©2022 Maxar Technologies.)

especially to coastal infrastructure. Various equipment was utilized to characterize and quantify storm impacts, including UAVs and TLS. A TDMS in Grand Isle was of particular interest, and the UAV and TLS surveys conducted at this location are the primary focus of the deployment for this study. Figure 1 illustrates the survey locations, the TDMS, and the path of the centre of Hurricane Ida, overlaid with the satellite and airborne imagery employed in this study.

2.2. Instrumentation and data collection

To assess large-scale vegetative debris transportation and quantities following Hurricane Ida, Sentinel-2 satellite imagery covering the Barataria Basin was acquired from the Copernicus Open Access Hub. Sentinel-2 imagery was chosen because it has the highest spatial resolution among publicly available satellite imagery (10 m) and orbits frequently enough (5–10 days) to investigate pre- and post-hazard conditions of the observed land. Publicly available imagery was selected because it is easily and openly accessible to everyone, making it more practical to emergency management officials and local governments with a limited amount of resources for disaster management, which is quite often the case (Jalloul et al. 2022). Demonstrating that publicly available imagery is applicable validates that fee-based imagery would also be. Imagery collected on 5 August 2021 was utilized to assess pre-hazard conditions and imagery collected on 19 October 2021 was employed for post-hazard conditions. Imagery was selected on these days because they

showed the least amount of cloud cover closest to the landfall of Hurricane Ida. The Sentinel-2 imagery was trimmed to exclude clouds as much as possible and focus primarily on Barataria Bay and surrounding communities up to the city of New Orleans (colourized map in Figure 1).

To further investigate vegetative debris transportation and quantities, emergency response airborne imagery collected on August 30 through 2 September 2021 by the NOAA Remote Sensing Division was employed. This imagery was chosen due to its public availability, high spatial resolution (15–30 cm), and acquisition immediately following the landfall of Hurricane Ida. The NOAA imagery (colourized, rectangular swaths in Figure 1) covers areas that support NOAA interests including safety of navigation, hazardous spills, marine debris impacts, and impacts to coastal zone management interests (NOAA 2022), and thus does not encompass the entire area that Sentinel-2 imagery covers.

A UAV survey was conducted over a TDMS in Grand Isle on 14 October 2021 to calculate disaster debris volumes. A DJI Matrice 210 equipped with a MicaSense Altum multispectral sensor was utilized to capture aerial imagery to be processed into a point cloud using SfM photogrammetry techniques. The UAV survey was planned using Pix4Dcapture, a commercial software application developed for creating and executing autonomous UAV flight plans. A DJI Matrice 210 was flown in a grid pattern of parallel flight lines with 80% frontal overlap and 70% side overlap from an approximate altitude of 40 m and a camera angle set at 70°, resulting in a Ground Sampling Distance (GSD) of 1.85 cm/pixel and the collection of 1,620 images. Images were geotagged during capture through the UAV's on-board GPS. To improve georeferencing, three ground control points (GCPs) were placed around the debris piles, surveyed with a Leica GS18 T GNSS RTK rover. A base station was set up at the beginning of the day to record positional information with more accurate triangulation. The GNSS RTK rover remained on GCPs for 8 minutes to collect corrections from the base station and calculate the position measurements. Figure 2 shows the GCP surveying (Figure 2a) and their locations (Figure 2b).

A TLS survey was conducted over the TDMS at the same time as the UAV survey to calculate disaster debris volumes and compare the results to the UAV data. The Leica

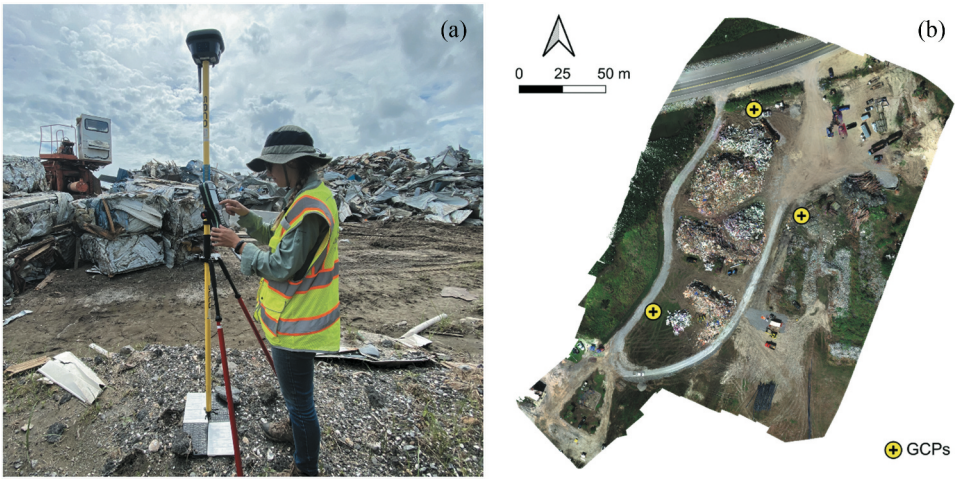

Figure 2. UAV data collection: (a) GCP surveying; and (b) their locations.

RTC360 3D Laser Scanner was employed to capture full 360° scans at close range (<65 m) to develop a high-resolution point cloud. The TLS survey was executed using Cyclone FIELD 360, a mobile-device application developed for use with the Leica RTC360 to link the point cloud data directly in the field and provide immediate data visualization. The TLS survey was conducted using a high point density mode (3 mm resolution at 10 m distance up to a range of 65 m). Point cloud resolution decreases as range increases and can vary substantially across the area due to obstructions and further objects, which increase noise. The decrease in resolution at further ranges is resolved by moving the scanner around the area of interest and taking multiple scans that are initially aligned in the field and validated in the processing stage. In this case, 15 total scans were taken at the TDMS. Figure 3 shows the Leica RTC360 during one of the scans (Figure 3a) and an image of the site captured by the Leica RTC360 (Figure 3b).

2.3. Data processing and debris quantification

To quantify vegetative debris created by Hurricane Ida across Barataria Basin as a result of coastal wetland loss, supervised image classification using a Support Vector Machine (SVM) algorithm was performed on the pre- and post-Ida Sentinel-2 imagery in ArcGIS Pro. SVM constructs a decision boundary, or hyperplane, that optimally separates different classes based on pixel value. Training data containing manually labelled pixels are provided to the algorithm along with the image to be classified. The algorithm then finds an optimal hyperplane in an iterative manner until a maximum margin is achieved, which is the distance between the hyperplane and the nearest data point from each class. False colour imagery in the form of near infrared, red, and green spectral bands mapped to the RGB colour space was utilized because it allows vegetation to be easily distinguished from water and other surroundings by the human eye, assisting classification of training and validation samples. Training and validation samples were collected from the Sentinel-2 imagery across two classes, land and water, via stratified random sampling and accuracy assessments were performed. Evident misclassified pixels were manually reclassified and accuracy assessments were performed on the reclassified maps. Vegetative debris generated was roughly estimated as the change in land area between the pre- and post-Ida imagery.

To determine the quantities and locations of transported vegetative debris, areas with vegetative debris in the NOAA imagery were identified and delineated in QGIS open-

Figure 3. TLS data collection: (a) TLS during scan; and (b) image of site captured via TLS.

source software, with a main focus on navigation networks, such as roads and waterways, infrastructure, and locations that would require debris removal. The delineated vegetative debris locations are limited to the coverage of the NOAA imagery. However, the NOAA imagery primarily covers towns and transportation networks, making it suitable for this analysis.

UAV image processing was executed using SfM photogrammetry techniques in Pix4Dmapper. SfM photogrammetry utilizes the camera position and orientation of each image collected and distinct features or keypoints to extract and match features that are recognizable in multiple images. Using the matched features and known position and orientation of the camera in each image, the software estimates the 3D coordinates of the matched features by triangulation. Bundle adjustment is performed, which iteratively minimizes errors in the estimated camera positions and feature locations through camera self-calibration. Camera self-calibration refines the intrinsic parameters and poses of the camera during each iteration to improve the overall consistency and accuracy of the 3D reconstruction. After bundle adjustment and camera self-calibration, the software generates a point cloud by interpolating between the 3D coordinates and additionally an orthomosaic of the imagery. To use the GCPs in the UAV imagery processing, base station coordinates were first corrected using the On-line Positioning User Service from the National Geodetic Survey, which provides free access to high-accuracy National Spatial Reference System Coordinates. The corrected base station position was used to compute a post-processed phase-fixed solution of the rover points, resulting in a 3D coordinate quality of 0.2 mm. The post-processed coordinates were loaded into the software to improve georeferencing of the model. A root mean square error of 0.6 cm was reported corresponding to the difference between the PPK measured coordinates of the GCPs and their calculated position in the reconstructed model based on their marking in images in the software. This value serves as a local indicator of how well Pix4Dmapper fitted the model to the GCPs. At a GSD of 1.85 cm/pixel and with the placement of GCPs, the maximum range of accuracy is estimated to be within 1.8–5.5 cm. This range is sufficient for disaster debris quantification applications, and thus does not affect our study's findings. The imagery covers approximately 38,000 m^2 and four separate debris piles. To calculate disaster debris pile volumes, the UAV point cloud was analysed in CloudCompare open-source software. The debris piles were segmented into four individual piles and 3D meshes were created for each segmented point cloud to compute the volume of each pile. A 3D mesh consists of a collection of vertices, edges, and faces that is generated based on the points within a point cloud and defines the shape and structure of a three-dimensional object. The volumes for each pile are the summation of the volumes of each individual polygon in the 3D mesh using its base and height. Height is calculated as the difference between the horizontal plane at the base of the debris pile (ground level) and the z-coordinate of the vertex.

To process the TLS data, Cyclone REGISTER 360 was utilized to register all captured scans together to create one composite point cloud. During this process, the alignments created in the field using Cyclone FIELD 360 were reviewed and adjusted as needed, the composite point cloud was colourized, and any mixed or oversaturated pixels were filtered out. A point cloud with 1 cm resolution was generated in addition to the 3 mm point cloud to facilitate point cloud rendering due to the high computational demands of the 3 mm point cloud. Similar to the

UAV point cloud, the TLS point cloud was analysed and segmented into four individual debris piles in CloudCompare and the volume of each debris pile was calculated based on the 3D mesh created for each segmented debris pile. Figure 4 presents the methodologies for quantifying disaster debris using satellite imagery, emergency response airborne imagery, UAV imagery, and TLS, respectively.

3. Results

Figure 5 presents the pre-Ida false colour Sentinel-2 satellite imagery collected on 5 August 2021 (Figure 5a), the post-Ida imagery collected on 19 October 2021 (Figure 5b), and the 19 October 2021 classification map overlaid with the change in land cover from 5 August 2021 (Figure 5c). The classification accuracy for both pre- and

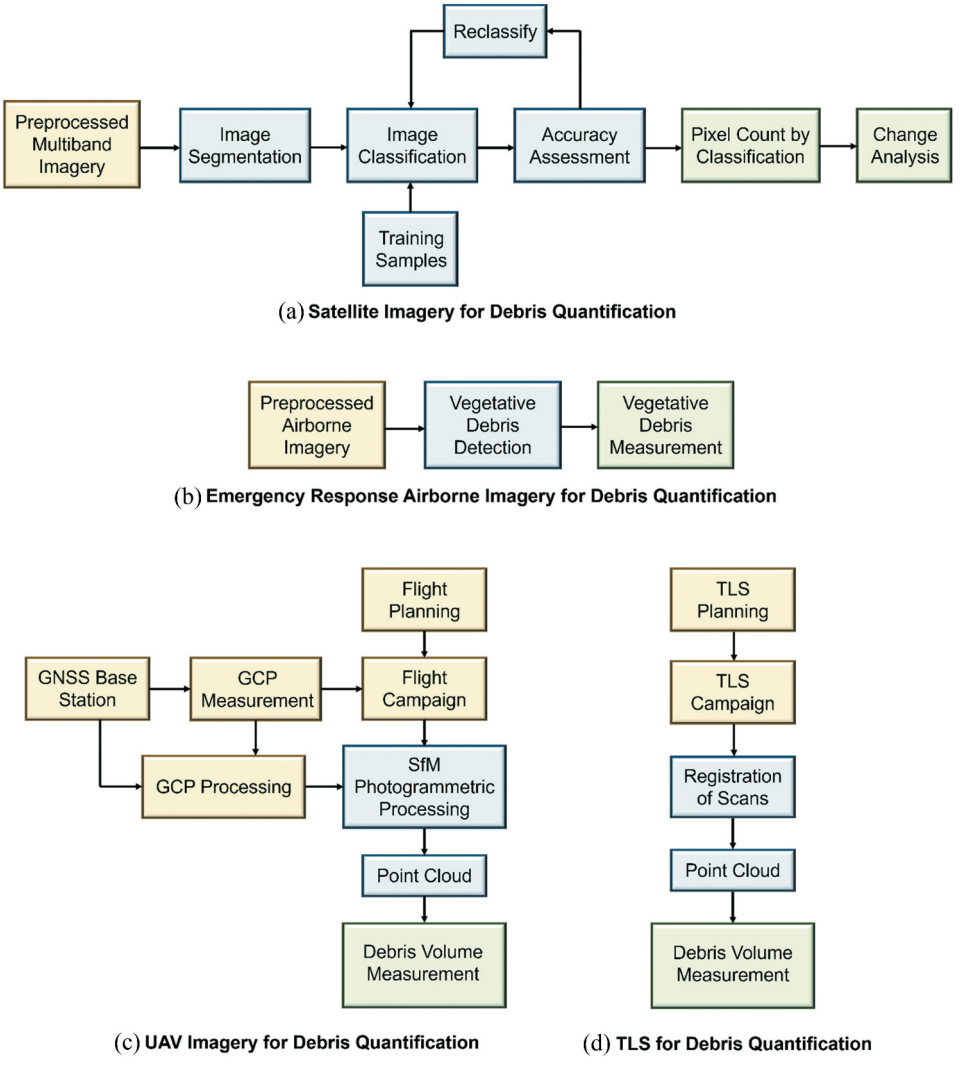

Figure 4. Workflow for debris quantification using multiple remote sensing tools. Data collection steps are yellow, data processing steps are blue, and debris quantification steps are green.

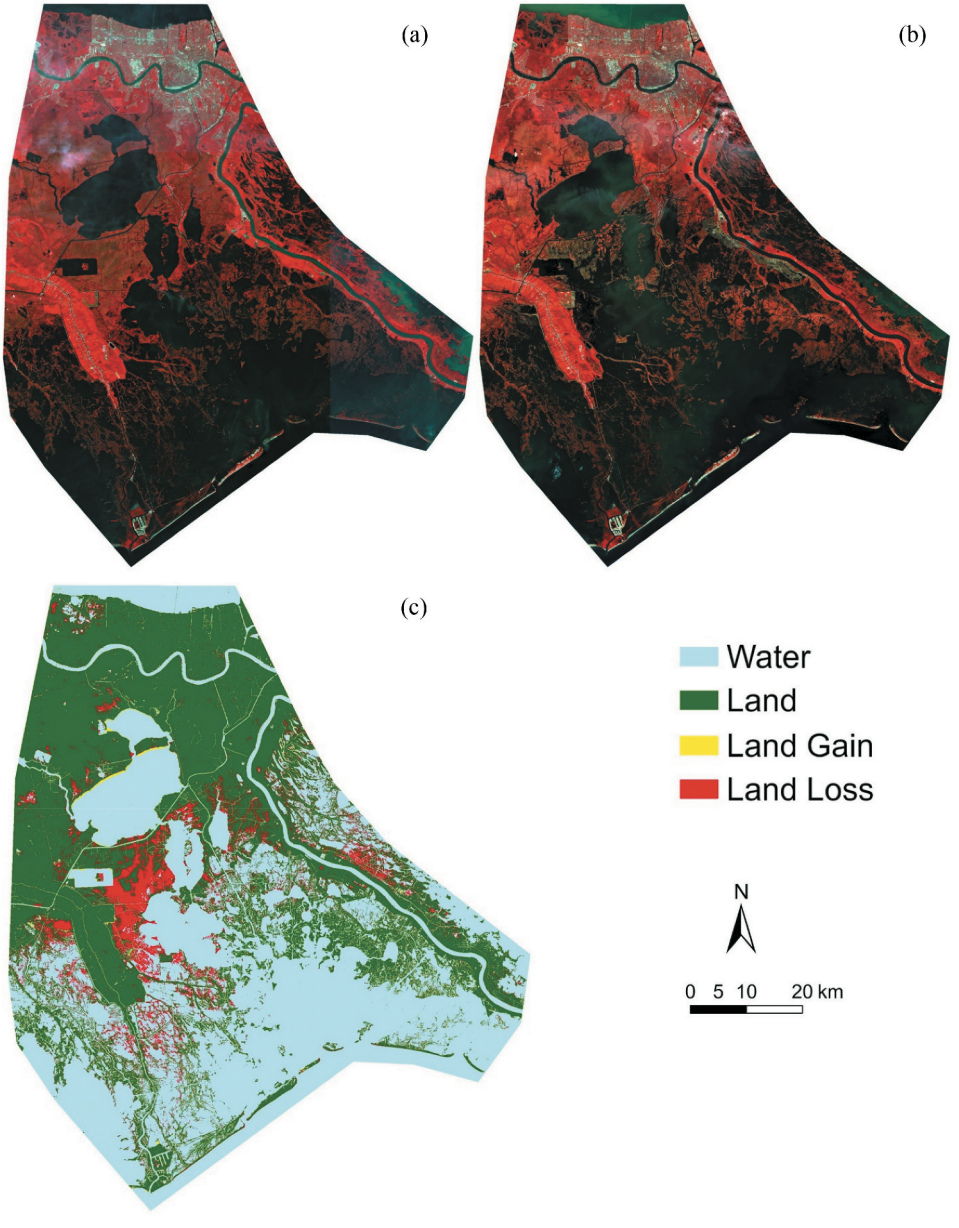

Figure 5. Sentinel-2 imagery: (a) false colour pre-Ida (08/05/21); (b) false colour post-Ida (10/19/21); (c) 10/19/21 classification map overlaid with change in land cover from 08/05/21.

post-Ida imagery was estimated at 96% based on 500 stratified random samples. The high accuracy is likely contributed to having only two classes, land and water, in the classification maps. The distribution of land cover change is illustrated in Figure 5c. Land loss is significant in northwest Barataria Bay, which overlaps with the occurrence of peak surge and waves. Land gain is noticeable on lakeshores northwest of Barataria Bay. The difference in land class pixels between the pre-Ida and post-Ida classification maps translate to

an approximate area of 329 km^2 of vegetative debris generated and transported elsewhere. A preliminary USGS study conducted following Hurricane Ida reported the loss of approximately 274 km^2 (106 mi^2) of wetlands in the Barataria Bay region (Schleifstein 2021). There are likely many reasons for the difference in these quantities, one of which is different spatial coverages. The imagery employed for this study has a spatial coverage of approximately 6,392 km^2, which appears larger than the coverage in the images presented in Schleifstein (2021). There may also be sources of uncertainty in this study's estimate, such as the resolution, cloud cover, shadows, and map accuracies. The 10 m resolution of the imagery illustrates that one misclassified pixel creates an error of 100 m^2. Cloud cover, which is apparent in Figure 5(a, b), also affects the classifications and can result in misclassified pixels. Although the accuracy of both classification maps is high at 96%, the accuracies are based on 500 random samples. Increasing training samples across the region could reduce misclassifications.

The NOAA emergency response airborne imagery surrounding Barataria Bay and delineations of vegetative debris requiring immediate removal are presented in Figure 6, along with Hurricane Ida's track. Figure 7 illustrates areas identified in Figure 6 with vegetative debris blocking infrastructure and transportation networks. Transported vegetative debris was not found in imagery north of Lake Salvador (Figure 6). Located west of Barataria Bay are multiple communities, including Golden Meadow (Figure 6), that have various flood protection infrastructure that forms a polder. This appeared to protect

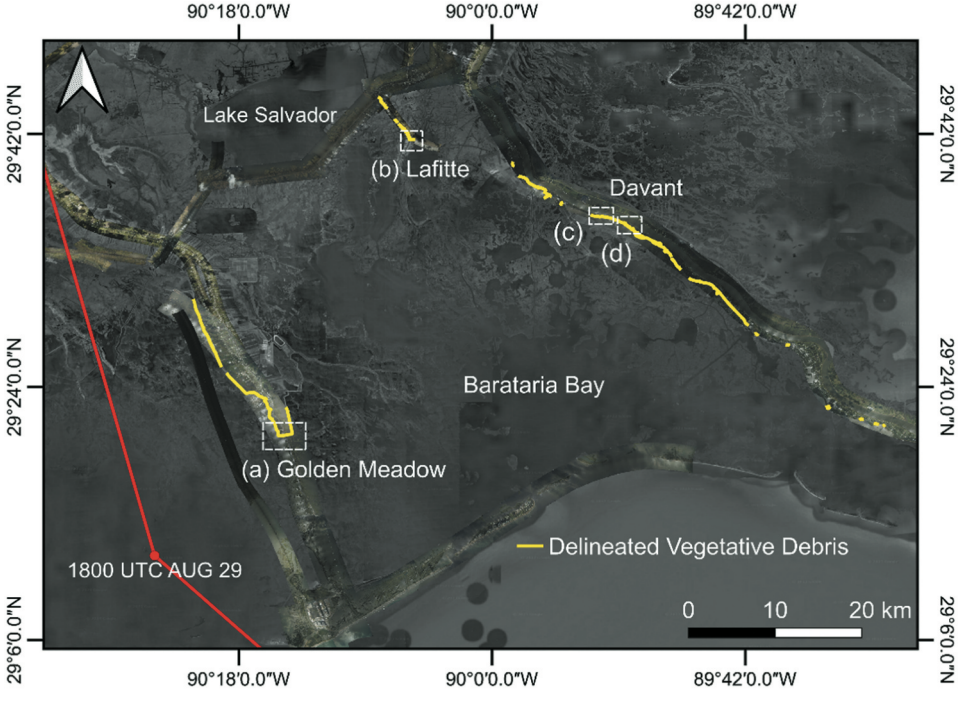

Figure 6. NOAA imagery with vegetative debris locations outlined and the time-stamped (UTC) path of the center of Hurricane Ida. Areas labelled a – d in Figure 6 are enlarged in Figure 7 and illustrate locations with large amounts of vegetative debris on infrastructure (Basemap: ©2022 Maxar Technologies.)

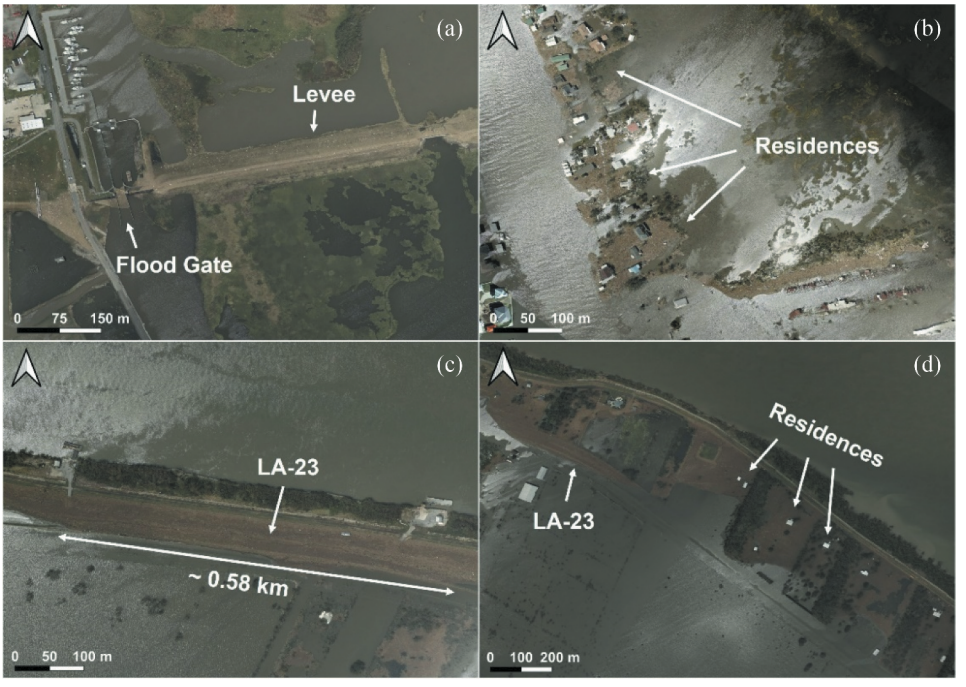

Figure 7. Areas within white boxes in Figure 6, following the same labelling and illustrating vegetative debris blocking: (a) levees and flood protection in Golden Meadow; (b) residential homes and infrastructure in Lafitte; and (c-d) roads and residential homes in Davant.

the communities from collecting vegetative debris, as debris was only found on the flood side (Figure 7a). North of Barataria Bay, vegetative debris was found piled against sheet pile walls. Vegetative debris was found to be especially prominent in Lafitte (Figure 6), where vegetative debris overtopped the seawalls and loaded on residential homes and infrastructure (Figure 7b). Communities east of Barataria Bay experienced the most instances of vegetative debris on infrastructure and transportation networks. Figures 7 (c, d), located in Davant (Figure 6), illustrate the severity of the transported vegetative debris. Figure 7c shows at least 0.58 km of Louisiana Highway 23 (LA-23) completely encompassed in vegetative debris, and Figure 7d shows another portion of LA-23 blocked and numerous residences entirely surrounded by vegetative debris. The severity of transported vegetative debris with respect to its impacts on infrastructure and transportation networks appears to be the greatest east of Barataria Bay, which ultimately affects the recovery time for these communities and individuals.

The orthomosaic produced from the UAV imagery is presented in Figure 8 (Figure 8a), along with the segmented point cloud (Figure 8b) and 3D meshes with debris piles labelled and coloured by height (Figure 8c). Height is relative to the ground surface which was set to zero. A histogram on the right of the colour scale indicates the proportion of points at each height. The UAV point cloud consists of 5,936,585 points, with a mean point cloud density of 173.88 points/m^2. The volumes calculated for debris piles 1, 2, 3, and 4 are 4,238 m^3, 3,509 m^3, 167 m^3, and 1,080 m^3, respectively. This imagery was collected on 14 October 2021, demonstrating that approximately 8,994 m^3 of disaster debris was collected and staged at this site

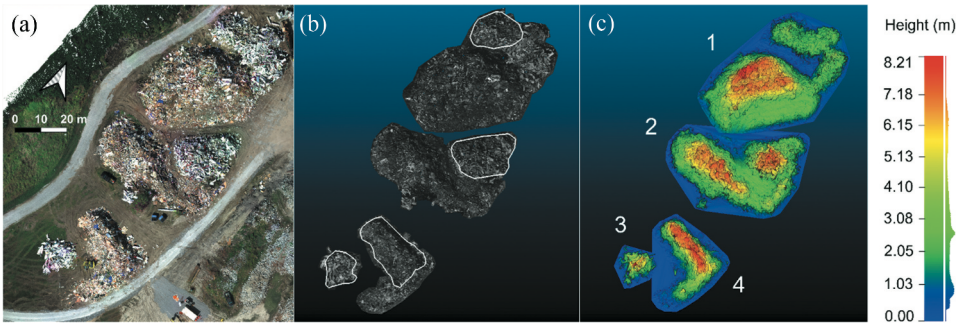

Figure 8. UAV Imagery: (a) orthomosaic; (b) segmented point cloud with white outlines around subsections extracted for analysis; and (c) 3D meshes with debris piles labelled and coloured by height.

over 46 days following Hurricane Ida's landfall on August 29. The debris is most likely all from Grand Isle due to its location at the entrance of the island (see Figure 1) and the fact that debris is likely not being brought from inland to the island. Thus, on average ~196 m^3/day was collected from Grand Isle and brought to this TDMS.

The point cloud produced from the TLS survey is presented in Figure 9 (Figure 9a), along with the segmented point cloud (Figure 9b) and 3D meshes with debris piles labelled and coloured by relative elevation (Figure 9c). Height was established in the same manner as the UAV point cloud. The TLS point cloud scaled to 1 cm resolution consists of 92,972,859 points, with a mean point cloud density of 6,100 points/m^2. The volumes calculated for debris piles 1, 2, 3, and 4 are 4,978 m^3, 3,726 m^3, 183 m^3, and 1,091 m^3, respectively. Gaps with missing data are apparent in the point cloud – primarily in debris piles 1 and 2 (Figure 9b). Using the UAV point cloud for reference, the gaps appear to be located in pile locations where the exterior is taller than the interior or there are obstructions. This is likely a consequence of the TLS survey being conducted on the ground and unable to scan through obstructions.

To directly compare UAV and TLS, subsections of debris piles without data gaps were extracted in both point clouds (white outlines in Figures 8 and 9). Figure 10 compares debris pile volumes derived from the UAV and TLS point clouds for both the entire piles (Figure 10a) and just the extracted subsections (Figure 10b). Figure 10a reveals differences in UAV and TLS

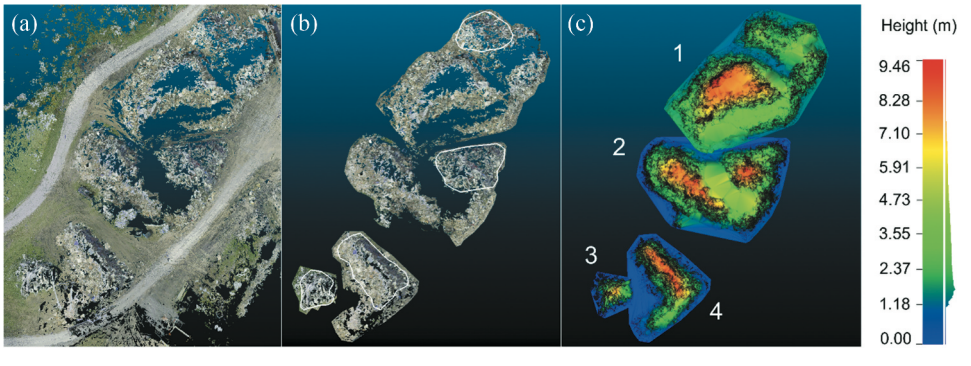

Figure 9. TLS Point Cloud: (a) composite point cloud; (b) segmented point cloud with white outlines around subsections extracted for analysis; and (c) 3D meshes with debris piles labelled and coloured by height.

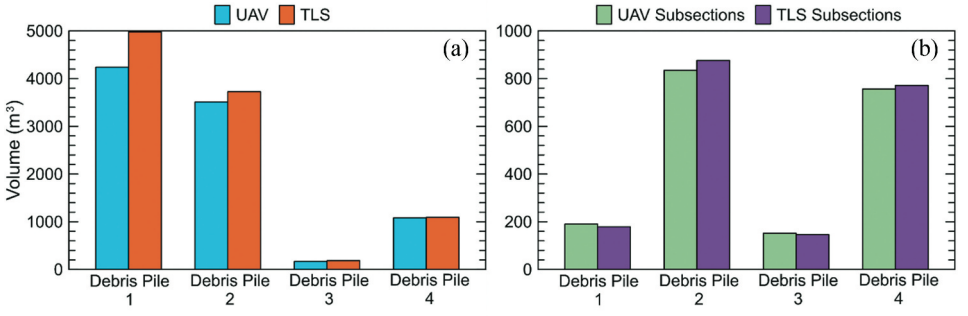

Figure 10. UAV and TLS debris volume comparisons: (a) entire debris piles; and (b) subsections within white outlines in Figure 8(b) and Figure 9(b).

computed volumes ranged from 1% to 16%, with an average of 8%. These disparities may stem from variations in the segmented debris pile boundaries between the UAV and TLS point clouds, which were segmented independently. The surface area of the segmented UAV point cloud is 4,484 m^2, whereas the surface area of the TLS point cloud is 4,714 m^2. Additionally, CloudCompare's interpolation method may inaccurately capture elevation gradients across TLS data gaps, assuming a near-constant elevation, while the UAV point cloud exhibits varying elevations in these gaps (see Figures 8 and 9). This could explain the higher debris volumes in the TLS point cloud. In the subsections, the differences in UAV and TLS computed volumes ranged from 2% to 6%, with an average of 4%. The differences only range from 6 to 42 m^3, which is relatively small in the context of disaster debris. Independent topography surveys conducted before and after the UAV and TLS surveys would allow for an accuracy assessment, but due to the lack of such data during disaster debris collection, this information is unavailable.

4. Discussion

Effective disaster debris management requires a reasonable understanding of the locations and quantities of debris generated by a disaster. This assists emergency management officials and local governments in all phases of a disaster and allows communities to promptly return to normal. This is becoming more important with the increasing prevalence of extreme events and their resulting disasters (CRED 2022). Remote sensing tools can provide valuable initial estimates of disaster debris quantities, offer insights into the spatial distribution of debris, and track the evolution of debris accumulation. Possible discrepancies between disaster debris estimates from remote sensing tools and statistical models can arise due to many factors, such as data sources and constraints, debris types, temporal and spatial resolutions, and model accuracy. By comparing remote sensing estimates with statistical model predictions, discrepancies can be identified and used to refine the model's parameters and assumptions, guide the adaptation of statistical models over time, and help keep statistical models current and responsive to changing conditions. This can be extremely valuable for emergency management officials and local governments that have limited technological resources.

Based on the debris quantification demonstrations, Figure 11 summarizes the performance of each remote sensing tool with respect to the following metrics: time for fieldwork, time for processing raw data, time for quantitative analyses, spatial coverage, spatial resolution, temporal resolution, cost, and operational effort. Relative values of highest,

	Satellite Imagery	Emergency Response Airborne Imagery	UAV	TLS
Time – Fieldwork	None	None	Medium Setting and surveying GCPs*, Flying UAV *If UAV without PPK/RTK Solutions	Medium Setups, Scan Times
Time – Processing Raw Data	Low < 1hr processed data	Low < 1hr processed data	Medium Regular Desktop = 3-5 hrs High-Performance Desktop =1-2 hrs	Medium Regular Desktop = 3-5 hrs High-Performance Desktop = 1-2 hrs
Time – Quantitative Analyses	Medium Training = 10 – 15 hrs Analyses = < 0.5 hr	Medium Manual Classification = 10 –15 hrs	Low	Low* *If scaled to lower resolution.
Spatial Coverage	High 1,000s km^2	Medium 100s km^2	Low Fixed-wing = 0-2 km^2 Quadcopter = 0-0.3 km^2	Low 0-0.5 km^2
Spatial Resolution	Low Public = 10 m Commercial = 1-3 m	Medium 15-30 cm	High 0-2 cm	Highest 3 mm
Temporal Resolution	Low 5 – 10 days	Medium Post-Disaster (1-5 days after disaster)	High User defined	High User defined
Cost	None* *Public - Free	None* *Public – Free	High Quadcopter = $1,000 - $2,000; $5,000 - $15,000 Fixed-wing = $15,000 - $20,000	Highest $20,000 - >$100,000
Operational Effort	Low	Low	High	Medium

Figure 11. Summary of criteria for each remote sensing technology for debris quantification. Metrics are categorized into different colour groups based on similarities and colour hues correspond to the magnitude of the results.

high, medium, low, or none were assigned for each tool and metric based on their performance. Thus, Figure 11 serves as a guide for selecting a remote sensing tool for debris quantification based on the desired application and available resources.

Satellite imagery can be useful for quantifying vegetative debris generated across vast areas by identifying areas where vegetation from wetlands has been relocated, such as

lakeshores and canals, as well as across the broader landscape. This can help identify priority areas for restoration efforts in areas like coastal Louisiana that experience intense land loss and high storm frequency. An advantage of satellite imagery is that it requires no fieldwork or deployments to collect the imagery, and both raw and pre-processed imagery can be publicly available, allowing for much less time spent collecting and processing the imagery. The most time is spent performing image classification to quantify debris, which was also found in Jiang and Friedland (2016). The Sentinel-2 satellite collects imagery across the world every 5–10 days, making it possible to download 1,000s km^2 of imagery at a time. However, with regard to debris quantification it is limited by spatial and temporal resolutions and unable to adequately detect debris at smaller scales (e.g. transportation networks, TDMS, and landfills). Satellite imagery is also prone to cloud cover, which makes it difficult to obtain cloudless imagery near a storm's landfall and adds uncertainty to debris quantification analyses. Conversely, imagery collected soon after hurricane landfall may have many areas with storm surge floodwater, resulting in inaccurate estimates of land lost versus inundated land (Schleifstein 2021). Satellite imagery with better spatial and temporal resolutions is available from commercial satellites. Jiang and Friedland (2016) and Shirai et al. (2016) utilize higher-resolution commercial satellite imagery (1–2 m) to estimate building damage debris zones, which was effective for their goals. However, commercial imagery comes at a cost of 14–25 USD/km^2 depending on the commercial agency (AAAS 2022). This may be reasonable for smaller study areas but may become quite expensive for larger study areas, such as the area employed in this study. Additionally, emergency management officials and local governments may have a limited amount of resources available to them for disaster management, especially for disaster debris specifically (Jalloul et al. 2022). Validating the applicability of publicly accessible imagery demonstrates that fee-based imagery, with its higher resolution, will also be applicable and perform better. As a result, it is suggested that agencies capable of acquiring fee-based imagery would do so. However, fee-based imagery with higher spatial resolutions may require more rigorous but time-consuming approaches, such as object-based image classification. Sentinel-2 satellite imagery does not appear to be the most effective remote sensing tool for debris quantification. However, depending on available resources, commercial satellite imagery may be more effective given computing time trade-offs.

Emergency response airborne imagery is suitable for identifying areas that require debris clearance to facilitate the provision of emergency services and locations that will need more debris removal and management resources. Multiple studies have effectively employed it for debris identification or quantification in combination with other data, such as panchromatic satellite imagery (Jiang and Friedland 2016), statistical modelling and field measurements (Szantoi et al. 2012), and airborne lidar (Hansen et al. 2007). Similar to satellite imagery, no fieldwork is required by the user to obtain the imagery. Emergency response airborne imagery is typically collected by government agencies, in this case by NOAA. The imagery is mosaicked and orthorectified prior to download, allowing for little time spent processing the imagery. The most time is spent identifying and delineating debris requiring removal across the extent of the airborne imagery. An advantage of airborne imagery is its higher spatial resolution compared to public satellite imagery (15 cm vs. 10 m), validating its suitability for quantifying debris that requires removal, such as on transportation networks and emergency service routes. Although the

resolution may be fine enough to discern debris at TDMS, NOAA emergency response airborne imagery is only provided as processed orthomosaics that do not include the raw imagery or metadata that would allow for SfM photogrammetric processing for volume quantifications. Other sources of emergency response airborne imagery may provide such data. Additionally, TDMS may not be located in the coverage obtained by the acquiring agency. Emergency response airborne imagery has much lower spatial coverage than satellite imagery due to its specific acquisition for extreme event impacts and the interests of the acquiring agency. Emergency response airborne imagery is collected immediately following a disaster, often resulting in a better temporal resolution than satellite imagery in the post-disaster scenario. However, in the U.S.A. the NOAA Remote Sensing Division only collects airborne imagery post-disaster and no pre-event imagery is acquired from this source. Adequate pre-disaster images may be available in countries with more frequent airborne surveys. This imagery is publicly available at no cost and is typically acquired below cloud ceilings, resulting in cloudless aerial imagery. Thus, emergency response airborne imagery appears to be an effective remote sensing tool for debris quantification to assist debris clearance on emergency service routes but can be limited spatially and temporally to the acquiring agency's interests.

UAVs are highly effective for quantifying disaster debris volumes. Furthermore, they can be employed for pre- and post-disaster surveys. Due to their limited spatial coverage, survey areas need to be predetermined using satellite or airborne imagery or ground campaigns. In contrast to satellite and emergency response airborne imagery, UAVs require field deployments and the imagery requires more time spent processing. Volumes were computed based on the 3D meshes created for each debris pile point cloud, which was almost immediate. Some other approaches have been utilized to calculate waste volumes from UAV imagery, i.e. using digital elevation maps (Son et al. 2019) and Python-based algorithms (Yoo et al. 2017), although the methods are all nearly identical. Python-based algorithms serve as the backbone for CloudCompare functions and digital elevation maps are created from the point cloud generated from SfM photogrammetric processing. Although volume calculations in this study were almost immediate, the time for processing and quantification analyses is dependent on computational resources and regular desktops may require more time to render dense point clouds based on the available CPU, GPU, or RAM. UAV surveys have low spatial coverage compared to satellite and airborne imagery, but spatial coverage from UAVs is dependent on the type of UAV and available battery. A quadcopter UAV, which was used in this study, has much lower spatial coverage than a fixed-wing UAV due to the mechanics of a quadcopter compared to a fixed-wing. UAVs have high spatial resolutions, typically 1–2 cm, and surveys can be performed at any temporal resolution desired by the user. For example, depending on the size and type of UAV, a user can conduct daily UAV surveys at TDMS to determine the volume of debris being brought in each day, providing emergency management officials with knowledge of the precise volumes of debris being collected over time. This application was demonstrated in Saffarzadeh et al. (2017), who reported 10,258 m^3 stored at a TDMS one month after an earthquake and 17,417 m^3 less than 2 months later. These efforts can assist efficient allocation and deployment of debris management resources, such as providing guidance for how many trucks should be deployed for debris removal, how much land is required to continue storing the debris, and where operations can be improved in the midst of the disaster. UAV surveys can also

assist characterization of the primary debris streams being generated due to the ability to discern objects in the imagery.

A disadvantage of UAVs is that they can be significantly more expensive than satellite and airborne imagery, although this depends on the use and type of UAV. Quadcopter UAVs are available across a range of prices: they begin at 1,000–2,000 USD for multiple quadcopter models and quickly jump to a range of 5,000–15,000 USD. The prices increase as more features are desired, such as higher-quality cameras, alternating payloads, and georeferencing capabilities. The DJI Matrice 210 used in this study is priced at 15,000 USD (NSF NHERI RAPID Experimental Facility, pers. comm., 2023). The range of prices for fixed-wing UAVs are higher due to their large-scale mapping abilities and often range from 15,000 to 20,000 USD. UAVs require much more operational effort than satellite or emergency response airborne imagery, where the only effort was in data processing and quantification analyses. UAV surveys require a licenced remote pilot to operate the UAV, a visual observer to constantly keep sight of the UAV, and if a survey needs to be expedited, an additional person to place and survey GCPs. An advantage of UAVs is that the pilot can conduct the survey a short distance away from the study site, allowing flexibility for safe operations around debris collection trucks, heavy equipment, and debris waste that may also contain hazardous materials. This is especially advantageous for areas that are not accessible on the ground due to obstructions from damage or debris. However, there are airspace and permission considerations depending on the country and respective regulations, such as not flying near airports or over bystanders without their permission. Depending on the available services, these obstacles can be overcome, for example, through the use of unmanned traffic management systems that facilitate UAV flights in restricted zones. Nonetheless, UAVs appear to be a highly effective remote sensing tool for debris quantification when debris is piled at TDMS and can provide precise volumes.

Similar to UAVs, TLS is highly effective for quantifying debris and can additionally provide precise volumes. TLS requires a similar amount of time spent in the field, processing data, and quantifying debris as UAVs. However, rendering the TLS point cloud at full resolution requires more computational resources than the UAV imagery due to the much higher density of the TLS point cloud. This study used a scaled-down TLS point cloud (3 mm to 1 cm) to facilitate analyses due to available computational resources. Spatial coverage for TLS is similar to quadcopter UAVs, but it may have less complete coverage than a UAV survey based on obstructions (see Figures 8–9). Heavy equipment and machinery moving debris was also present during the survey, which may have contributed to poor scan registrations and gaps in the point cloud. TLS has the highest spatial resolution out of all methods (3 mm), which allows for significantly less uncertainty with regard to debris quantification and can assist debris characterization efforts. The higher resolution of the TLS point cloud has higher computational demands and may have trouble rendering on a regular computer setup. It should be noted that UAVs can still achieve millimetre resolution based on factors such as flight height, UAV model, and sensor type; however, centimetre level resolutions are the most common (Z. Zhang and Zhu 2023). TLS surveys can be performed at any temporal resolution desired by the user, making it another useful method for determining volumes of debris being brought in to TDMS each day.

A disadvantage of TLS is the high cost of the equipment. TLS equipment is significantly more expensive than all other remote sensing tools, ranging from

approximately 20,000 USD to greater than 100,000 USD. The Leica RTC360 used in this study is priced at 88,000 USD (NSF NHERI RAPID Experimental Facility, pers. comm., 2023). A TLS survey requires slightly less operational effort than a UAV survey, as GCPs are not critical for the purpose of debris quantification. If a UAV with RTK/PPK solutions was used, GCPs would not be necessary, further simplifying UAV operations. UAVs with RTK/PPK solutions and lidar sensors were not employed in this study because of their high cost and inaccessibility to the authors at the time of the disaster. These tools should also be explored because they may provide more accurate results at the expense of more data processing time. Even so, the conclusions of the study would remain true with or without these technologies. A TLS survey is performed on the ground, directly in front of the debris at the study area, which may not be feasible for obstructed areas. Similar to a UAV survey, there are permission considerations depending on the site. TLS appears to be an effective remote sensing tool for disaster debris quantification, as it can provide precise volumes of debris. However, it may not be as efficient as a UAV due to the cost and computational demands of TLS. An application TLS may be better suited for than UAVs is assessing building damage and resulting debris, which was effectively demonstrated in Berman et al. (2020) and Zaragoza et al. (2017). This is because a typical UAV survey may be limited to only damage visible from an aerial view.

Understanding the best applications of multiple remote sensing tools can assist decision making for emergency management officials and disaster waste managers interested in quantifying disaster debris. The comparisons and demonstrated workflows presented in this study can help emergency management officials decide which tool to employ based on their desired application and available resources. The metrics utilized in the comparisons may have different values to various users, and thus including multiple metrics allows users to choose a remote sensing tool based on the criteria and applications most important to them. A key finding of this study was that remote sensing tools can be employed for diverse applications with regard to disaster debris quantification. Additionally, the lack of information on post-disaster waste quantities can be effectively addressed using remote sensing tools. In particular, the UAV and TLS data in this study serve as examples by providing volume quantities of collected disaster debris. Future studies can employ these approaches together to conduct repeat surveys to determine debris generation over time. UAVs and TLS are easy to transport, making them well-suited for reconnaissance investigations to collect post-disaster waste data.

Based on the demonstrations and comparisons in this study, Figure 12 summarizes suitable applications of the remote sensing tools across the primary phases of disaster management (pre-disaster, response, recovery) and demonstrates how applications in one phase can inform the subsequent phase. The pre-disaster phase could be similar to the planning phase, but it is defined herein to also include the time pre-hazard (e.g. predictions of hurricanes, floods, sediment debris) such that perishable data collection can occur. In the pre-disaster phase, efforts are focused on planning for debris collection, forecasting potential debris quantities, and determining suitable locations for TDMS (FEMA 2007; USEPA 2019). Remote sensing tools employed in this stage will be most useful for determining TDMS locations and

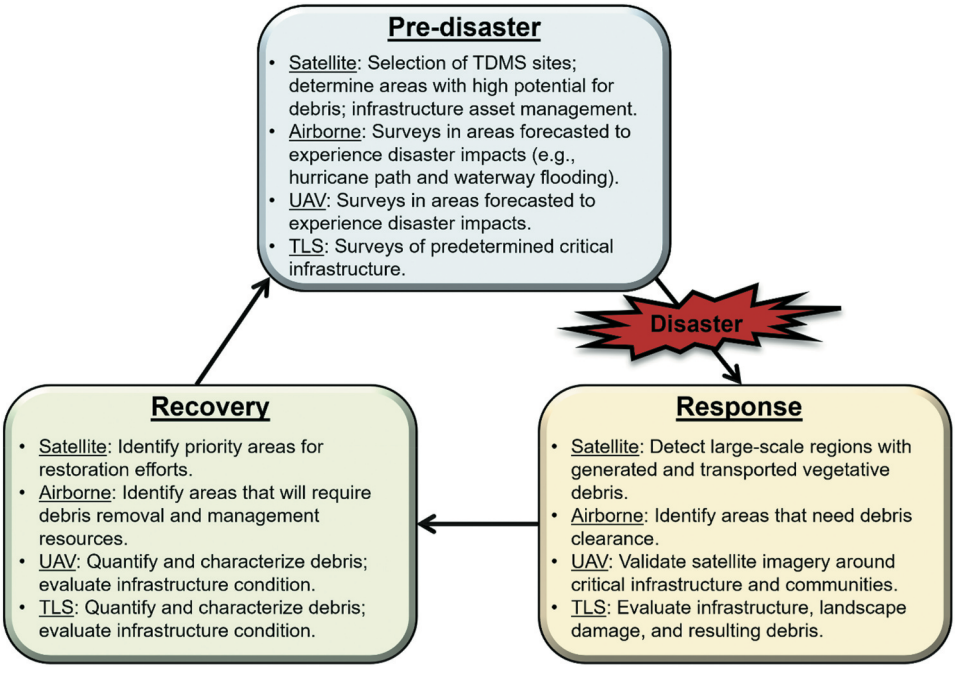

Figure 12. Suitable applications of remote sensing tools in different disaster management phases.

surveying sites forecasted to be impacted by the event, which will facilitate direct before and after comparisons. The response phase occurs immediately after an event and is primarily focused on clearing debris from emergency service routes (FEMA 2007). In this phase, remote sensing tools will be most beneficial for quantifying debris that must be removed to restore critical infrastructure and emergency service routes. The recovery phase begins once emergency service routes are cleared and debris is brought to public rights-of-way, collected, and transported to TDMS (FEMA 2007). Remote sensing tools utilized in this phase will be most useful for quantifying debris volumes and determining areas that may require more debris management resources, which can improve operations and speed up recovery. The applications of the remote sensing tools are not limited to those listed in Figure 12, but rather serve as suitable examples for emergency management officials, stakeholders, researchers, and users interested in quantifying disaster debris.

This study utilizes each remote sensing tool individually to address the knowledge gap on the performance, advantages, and shortcomings of each individual tool for disaster debris quantification. Through this approach, the results of the comparisons can not only help for selecting a tool but can guide future studies for combining multiple tools based on their performance, specifications, and application. Further studies that use remote sensing tools to quantify disaster debris are critical for validating the results of this study, especially studies that combine multiple tools to improve disaster debris estimates and mitigate discrepancies and uncertainty in the data.

5. Conclusions

The aim of this study was to demonstrate and compare multiple remote sensing tools available for quantifying disaster debris using post-disaster data collected following Hurricane Ida. These measures will assist disaster debris quantification and management efforts for future disasters. The results of this study found that satellite imagery is useful for identifying where vegetative debris was created and transported across expansive spatial areas, although publicly available imagery is limited by spatial and temporal resolutions. Emergency response airborne imagery is well-suited for quantifying transported vegetative debris and determining areas that need immediate debris management resources, such as emergency service routes that require debris clearance. However, it can be limited spatially and temporally to the interests of the acquiring agency. UAVs and TLS are highly effective for quantifying debris and can provide precise volumes. This provides emergency management officials with workflows for calculating debris volumes, which will contribute to the lack of data on post-disaster waste quantities. Furthermore, UAVs may be a better option for quantifying debris volumes rather than TLS due to their lower cost and computational demand. A framework was developed to evaluate remote sensing technologies and their efficacy in debris management, which will assist debris quantification efforts and decision making for disaster waste managers.

Funding

This work was supported by the National Science Foundation (NSF) through a Graduate Research Fellowship to Jasmine H. Bekkaye, through the Nearshore Extreme Event Reconnaissance Association (NEER) under Grant 1939275, and NSF as part of the RAPID Facility, a component of the Natural Hazards Engineering Research Infrastructure, under Grant 2130997.

Acknowledgements

The authors would like to thank the National Oceanic and Atmospheric Association (NOAA) and the European Space Agency (ESA) Copernicus Program for providing freely available data. The authors would also like to thank the RAPID Facility, a component of the National Science Foundation (NSF) Natural Hazards Engineering Research Infrastructure (NHERI), for providing the surveying, unmanned aerial vehicle, and terrestrial laser scanning equipment used in this study. In addition, this work was supported by the NSF through a Graduate Research Fellowship to Jasmine H. Bekkaye and through the Nearshore Extreme Event Reconnaissance Association (NEER). Any opinions, findings, and conclusions or recommendations expressed in this material are those of the author(s) and do not necessarily reflect the views of NSF.

Disclosure statement

No potential conflict of interest was reported by the author(s).

ORCID

Jasmine H. Bekkaye http://orcid.org/0000-0002-2027-1524
Navid H. Jafari http://orcid.org/0000-0002-4394-3776

Data Availability statement

The Sentinel-2 satellite imagery used in this study is freely available via the Copernicus Open Access Hub (https://dataspace.copernicus.eu/browser/) and the NOAA emergency response imagery is freely available via https://storms.ngs.noaa.gov/storms/ida/index.html#9/29.2029/-90.1932. All data collected during the joint NEER/GEER reconnaissance effort can be found in DesignSafe via https://doi.org/10.17603/ds2-8ks9-ag46.

References

AAAS (American Association for the Advancement of Science). 2022. "High-Resolution Satellite Imagery Ordering and Analysis Handbook." Accessed April 17, 2023. https://www.aaas.org/resources/high-resolution-satellite-imagery-ordering-and-analysis-handbook.

Axel, C., J. A. N. van Aardt, F. Aros-Vera, and J. Holguín-Veras. 2016. "Remote Sensing-Based Detection and Quantification of Roadway Debris Following Natural Disasters." *Proceedings of SPIE* 9832:98320C. https://doi.org/10.1117/12.2223073.

Bekkaye, J. H., and N. H. Jafari. 2023. "Flood Debris Quantification and Comparison Based on the Removal and Disposal Operation: Postdisaster Study of Beaumont, Texas Following Hurricane Harvey." *Natural Hazards Review* 24 (4). https://doi.org/10.1061/NHREFO.NHENG-1785.

Berman, J. W., J. Wartman, M. Olsen, J. L. Irish, S. B. Miles, T. Tanner, K. Gurley, et al. 2020. "Natural Hazards Reconnaissance with the NHERI RAPID Facility." *Frontiers in Built Environment* 6:573067. https://doi.org/10.3389/fbuil.2020.573067.

Beven, J. L.,II, A. Hagen, and R. Berg. 2022. "National Hurricane Center Tropical Cyclone Report: Hurricane Ida." Accessed April 20, 2023. https://www.nhc.noaa.gov/data/tcr/AL092021_Ida.pdf.

Brown, C., M. Milke, and E. Seville. 2011. "Disaster Waste Management: A Review Article." *Waste Management* 31 (6): 1085–1098. https://doi.org/10.1016/j.wasman.2011.01.027.

Chowdhury, T., M. Rahnemoonfar, R. Murphy, and O. Fernandes. 2020. "Comprehensive Semantic Segmentation on High Resolution UAV Imagery for Natural Disaster Damage Assessment." *Proceedings of 2020 IEEE International Conference on Big Data* 3904–3913. https://doi.org/10.1109/BigData50022.2020.9377916.

CRED (Center for Research on the Epidemiology of Disasters). 2022. "Disasters in Numbers 2021." Accessed March 21, 2023. https://reliefweb.int/report/world/2021-disasters-numbers.

Dai, K., A. Li, H. Zhang, S.-E. Chen, and Y. Pan. 2018. "Surface Damage Quantification of Postearthquake Building Based on Terrestrial Laser Scan Data." *Structural Control & Health Monitoring* 25 (8): 8. https://doi.org/10.1002/stc.2210.

Duarte, D., F. Nex, N. Kerle, and G. Vosselman. 2018. "Multi-Resolution Feature Fusion for Image Classification of Building Damages with Convolutional Neural Networks." *Remote Sensing* 10 (10): 1636. https://doi.org/10.3390/rs10101636.

FEMA (Federal Emergency Management Agency). 2007. *Public Assistance Debris Management Guide*. Washington, DC, USA: FEMA.

Filkin, T., N. Sliusar, M. Huber-Humer, M. Ritzkowski, and V. Korotaev. 2022. "Estimation of Dump and Landfill Waste Volumes Using Unmanned Aerial Systems." *Waste Management* 139:301–308. https://doi.org/10.1016/j.wasman.2021.12.029.

Ghaffarian, S., and N. Kerle. 2019. "Towards Post-Disaster Debris Identification for Precise Damage and Recovery Assessments from UAV and Satellite Images." *International Archives of the Photogrammetry, Remote Sensing and Spatial Information Sciences* XLII-2/W13:297–302. https://doi.org/10.5194/isprs-archives-XLII-2-W13-297-2019.

Hamdi, Z. M., M. Brandmeier, and C. Straub. 2019. "Forest Damage Assessment Using Deep Learning on High Resolution Remote Sensing Data." *Remote Sensing* 11 (17): 1976. https://doi.org/10.3390/rs11171976.

Hanifa, N. R., E. Gunawan, S. Firmansyah, L. Faizal, D. A. Retnowati, G. C. Pradipta, I. Imran, and J. A. Lassa. 2022. "Unmanned Aerial Vehicles for Geospatial Mapping of Damage Assessment: A Study Case of the 2021 Mw 6.2 Mamuju-Majene, Indonesia, Earthquake During the Coronavirus

Disease 2019 (COVID-19) Pandemic." *Remote Sensing Applications: Society & Environment* 28:100830. https://doi.org/10.1016/j.rsase.2022.100830.

Hansen, M., P. Howd, A. Sallenger, C. W. Wright, and J. Lillycrop. 2007. *Estimation of Post-Katrina Debris Volume: An Example from Coastal Mississippi*. Reston, Virginia, USA: US Geological Survey. https://doi.org/10.3133/cir13063e.

Hong, Z., H. Zhong, H. Pan, J. Liu, R. Zhou, Y. Zhang, Y. Han, J. Wang, S. Yang, and C. Zhong. 2022. "Classification of Building Damage Using a Novel Convolutional Neural Network Based on Post-Disaster Aerial Images." *Sensors* 22 (15): 5920. https://doi.org/10.3390/s22155920.

Jafari, N., S. S. C. Congress, A. Puppula, and H. M. Nazari. 2019. "RAPID Collaborative: Data Driven Post-Disaster Waste and Debris Volume Predictions Using Smartphone Photogrammetry App and Unmanned Aerial Vehicles." DesignSafe–CI. https://doi.org/10.17603/DS2TX26.

Jalloul, H., J. Choi, N. Yesiller, D. Manheim, and S. Derrible. 2022. "A Systematic Approach to Identify, Characterize, and Prioritize the Data Needs for Quantitative Sustainable Disaster Debris Management." *Resources, Conservation, and Recycling* 180:106174. https://doi.org/10.1016/j.resconrec.2022.106174.

Jiang, S., and C. J. Friedland. 2016. "Automatic Urban Debris Zone Extraction from Post-Hurricane Very High-Resolution Satellite and Aerial Imagery." *Geomatics, Natural Hazards and Risk* 7 (3): 933–952. https://doi.org/10.1080/19475705.2014.1003417.

Jiao, Q., H. Jiang, and Q. Li. 2019. "Building Earthquake Damage Analysis Using Terrestrial Laser Scanning Data." *Advances in Civil Engineering* 2019:8308104. https://doi.org/10.1155/2019/8308104.

Kakooei, M., and Y. Baleghi. 2017. "Fusion of Satellite, Aircraft, and UAV Data for Automatic Disaster Damage Assessment." *International Journal of Remote Sensing* 38 (8–10): 2511–2534. https://doi.org/10.1080/01431161.2017.1294780.

Koyama, C. N., H. Gokon, M. Jimbo, S. Koshimura, and M. Sato. 2016. "Disaster Debris Estimation Using High-Resolution Polarimetric Stereo-SAR." *ISPRS Journal of Photogrammetry and Remote Sensing* 120:84–98. https://doi.org/10.1016/j.isprsjprs.2016.08.003.

Labiak, R. C., J. A. N. van Aardt, D. Bespalov, D. Eychner, E. Wirch, and H.-P. Bischof. 2011. "Automated Method for Detection and Quantification of Building Damage and Debris Using Post-Disaster Lidar Data." *Proceedings of SPIE* 8037:80370F. https://doi.org/10.1117/12.883509.

Luther, L. 2017. "Disaster Debris Management, Requirements, Challenges, and Federal Agency Roles." Accessed March 15, 2023. https://sgp.fas.org/crs/homesec/R44941.pdf.

Marchesini, G., H. Beraud, and B. Barroca. 2021. "Quantification of Disaster Waste: Review of the Available Methods." *International Journal of Disaster Risk Reduction* 53:101996. https://doi.org/10.1016/j.ijdrr.2020.101996.

NASEM (National Academies of Sciences, Engineering, and Medicine). 2014. *A Debris Management Handbook for State and Local DOTs and Departments of Public Works*. Washington, DC, USA: The National Academies Press. https://doi.org/10.17226/22239.

NOAA (National Oceanic and Atmospheric Administration). 2022. "2022 U.S. Billion-Dollar Weather and Climate Disasters in Historical Context." Accessed April 27, 2023. https://www.climate.gov/news-features/blogs/2022-us-billion-dollar-weather-and-climate-disasters-historical-context.

Olsen, M. J., K. F. Cheung, Y. Yamazakl, S. Butcher, M. Garlock, S. Yim, S. McGarity, I. Robertson, L. Burgos, and Y. L. Young. 2012. "Damage Assessment of the 2010 Chile Earthquake and Tsunami Using Terrestrial Laser Scanning." *Earthquake Spectra* 28 (S1): 179–197. https://doi.org/10.1193/1.4000021.

Pham, T. T. H., P. Apparicio, C. Gomez, C. Weber, and D. Mathon. 2014. "Towards a Rapid Automatic Detection of Building Damage Using Remote Sensing for Disaster Management: The 2010 Haiti Earthquake." *Disaster Prevention & Management* 23 (1): 53–66. https://doi.org/10.1108/DPM-12-2012-0148.

Pi, Y., N. D. Nath, and A. H. Behzadan. 2020a. "Convolutional Neural Networks for Object Detection in Aerial Imagery for Disaster Response and Recovery." *Advanced Engineering Informatics* 43:101009. https://doi.org/10.1016/j.aei.2019.101009.

Pi, Y., N. D. Nath, and A. H. Behzadan. 2020b. "Detection and Semantic Segmentation of Disaster Damage in UAV Footage." *Journal of Computing in Civil Engineering* 35 (2). https://doi.org/10.1061/(ASCE)CP.1943-5487.0000947.

Saffarzadeh, A., T. Shimaoka, H. Nakayama, and S. A. Fard. 2019. "Lessons Learned from the Ezgeleh–Sarpol Zahab Earthquake of November 2017: Status of Damage and Disposal of Disaster Waste." *Waste Disposal & Sustainable Energy* 1 (4): 301–317. https://doi.org/10.1007/s42768-019-00025-9.

Saffarzadeh, A., T. Shimaoka, H. Nakayama, T. Hanashima, K. Yamaguchi, and K. Manabe. 2017. "Tasks and Problems Involved in the Handling of Disaster Waste Upon April 2016 Kumamoto Earthquake, Japan." *Natural Hazards* 89 (3): 1273–1290. https://doi.org/10.1007/s11069-017-3021-1.

Schleifstein, M. 2021. "Hurricane Ida Blamed for 'Incredibly Significant Loss of 106 Square Miles of Wetlands." Accessed May 24, 2023. https://www.nola.com/news/environment/hurricane-ida-blamed-for-incredibly-significant-loss-of-106-square-miles-of-wetlands/article_8b154c88-47f5-11ec-b558-e702c7d5d7da.html.

Shirai, H., Y. Kageyama, A. Ohuchi, and M. Nishida. 2016. 'Estimation of the Disaster Building Domain Using RapidEye Data to Estimate the Amount of Disaster Waste.' *IEEJ Transactions on Electrical and Electronic Engineering* 11 (S2): S53–S59. https://doi.org/10.1002/tee.22326.

Sliusar, N., T. Filkin, M. Huber-Humer, and M. Ritzkowski. 2022. "Drone Technology in Municipal Solid Waste Management and Landfilling: A Comprehensive Review." *Waste Management* 139:1–16. https://doi.org/10.1016/j.wasman.2021.12.006.

Son, S. W., J. H. Yoon, H. J. Jeon, D. W. Kim, and J. J. Yu. 2019. "Optimal Flight Parameters for Unmanned Aerial Vehicles Collecting Spatial Information for Estimating Large-Scale Waste Generation." *International Journal of Remote Sensing* 40 (20): 8010–8030. https://doi.org/10.1080/01431161.2019.1608387.

Szantoi, Z., S. Malone, F. Escobedo, O. Misas, S. Smith, and B. Dewitt. 2012. "A Tool for Rapid Post-Hurricane Urban Tree Debris Estimates Using High Resolution Aerial Imagery." *International Journal of Applied Earth Observation and Geoinformation* 18:548–556. https://doi.org/10.1016/j.jag.2011.10.009.

USEPA (U.S. Environmental Protection Agency). 2019. *Planning for natural disaster debris*. Washington, DC, USA: USEPA.

Wang, C., X. Qiu, H. Huan, S. Wang, Y. Zhang, X. Chen, and W. He. 2021. "Earthquake-Damaged Buildings Detection in Very High-Resolution Remote Sensing Images Based on Object Context and Boundary Enhanced Loss." *Remote Sensing* 13 (16): 3119. https://doi.org/10.3390/rs13163119.

Yeom, J., Y. Han, A. Chang, and J. Jung. 2019. "Hurricane Building Damage Assessment Using Post-Disaster UAV Data," In *Proceedings of 2019 IEEE International Symposium on Geoscience and Remote Sensing*, 9867–9870. https://doi.org/10.1109/IGARSS.2019.8900477.

Yoo, H. T., H. Lee, S. Chi, B.-G. Hwang, and J. Kim. 2017. "A Preliminary Study on Disaster Waste Detection and Volume Estimation Based on 3D Spatial Information." *Proceedings of Computing in Civil Engineering* 2017:428–435. https://doi.org/10.1061/9780784480823.051.

Zaragoza, I. M.-E., G. Caroti, A. Piemonte, B. Riedel, D. Tengen, and W. Niemeier. 2017. "Structure from Motion (SfM) Processing of UAV Images and Combination with Terrestrial Laser Scanning, Applied for a 3D-Documentation in a Hazardous Situation." *Geomatics, Natural Hazards and Risk* 8 (2): 1492–1504. https://doi.org/10.1080/19475705.2017.1345796.

Zhang, F., C. Cao, C. Li, Y. Liu, and D. Huisingh. 2019. "A Systematic Review of Recent Developments in Disaster Waste Management." *Journal of Cleaner Production* 235:822–840. https://doi.org/10.1016/j.jclepro.2019.06.229.

Zhang, Z., and L. Zhu. 2023. "A Review on Unmanned Aerial Vehicle Remote Sensing: Platforms, Sensors, Data Processing Methods, and Applications." *Drones* 7 (6): 398. https://doi.org/10.3390/drones7060398.